Geophysical Research Letters

RESEARCH LETTER
10.1029/2020GL089182

Common Mechanism for Interannual and Decadal Variability in the East African Long Rains

Dean P. Walker[1], John H. Marsham[1,2], Cathryn E. Birch[1], Adam A. Scaife[3,4], and Declan L. Finney[1]

[1]School of Earth and Environment, University of Leeds, Leeds, UK, [2]National Centre for Atmospheric Science, Leeds, UK, [3]Met Office Hadley Centre, Exeter, UK, [4]College of Engineering, Mathematics and Physical Sciences, University of Exeter, Exeter, UK

Key Points:
- East African long rains interannual and decadal variability have the same quantitative link to winds across the Congo and Gulf of Guinea
- Drier long rains and the corresponding zonal wind anomalies are linked to Sahelian warming on both interannual and decadal time scales
- The Madden-Julian Oscillation influences both the zonal winds and the long rains on interannual and decadal time scales

Supporting Information:
- Supporting Information S1

Correspondence to:
D. P. Walker,
eedpw@leeds.ac.uk

Citation:
Walker, D. P., Marsham, J. H., Birch, C. E., Scaife, A. A., & Finney, D. L. (2020). Common mechanism for interannual and decadal variability in the East African long rains. *Geophysical Research Letters*, *47*, e2020GL089182. https://doi.org/10.1029/2020GL089182

Received 16 JUN 2020
Accepted 17 OCT 2020
Accepted article online 26 OCT 2020

©2020. The Authors.
This is an open access article under the terms of the Creative Commons Attribution License, which permits use, distribution and reproduction in any medium, provided the original work is properly cited.

Abstract The East African long rains constitute the main crop-growing season in the region. Interannual predictability of this season is low in comparison to the short rains, and recent decadal drying contrasts with climate projections of a wetter future (the "East African climate paradox"). Here, we show that long rains rainfall totals are strongly correlated with 700 hPa zonal winds across the Congo basin and Gulf of Guinea ($r = 0.73$). Westerly anomalies align with more rainfall, with the same mechanism controlling covariability on interannual and decadal time scales. On both time scales wind anomalies are linked to geopotential anomalies over the Sahel and Sahara, and warming there. Rainfall and wind are significantly correlated with the Madden-Julian Oscillation (MJO) amplitude, and around 18% of the decadal drying can be explained by MJO amplitude variability. This work shows that predictions of East African rainfall across time scales require robust prediction of both zonal winds and MJO activity.

Plain Language Summary East Africa has two rainfall seasons, the main season, the long rains, runs from March to May. There is currently little understanding of what controls the amount of rainfall during this season. Recent drying, causing many areas to suffer from droughts and food shortages, contrasts with climate projections of a wetter future (the "East African climate paradox"). Rainfall is found to be connected to the strength of easterly winds over the Congo basin and Gulf of Guinea, with the same mechanism controlling variability on both interannual and decadal time scales. From 1998 to 2011 the winds had been getting stronger, with reduced rainfall over East Africa. The cause of the stronger wind is investigated and is partly explained by relatively fast warming in the Sahel than over the Congo, while variation in Madden-Julian Oscillation (a large-scale tropical wave) activity, explains around 18% of the decadal drying.

1. Introduction

Equatorial East Africa has two rainfall seasons per year, the long rains, occurring March-May (MAM), and short rains, occurring October-December (OND). A large contrast in the predictability of the two seasons has been observed (Batté & Déqué, 2011; Camberlin & Philippon, 2002; Dutra et al., 2013; Nicholson, 2017; Walker et al., 2019). This has been attributed to the short rains being influenced by global-scale modes of variability such as El Niño–Southern Oscillation (Indeje et al., 2000; Nicholson & Entekhabi, 1986), and the Indian Ocean Dipole (Black et al., 2003; Saji et al., 1999), while such relationships are absent during the long rains (Ogallo, 1988).

In most areas of equatorial East Africa, the long rains is the main crop growing season, generally providing greater (Camberlin & Wairoto, 1997), and more reliable (Camberlin & Philippon, 2002), rainfall amounts. However, in recent decades there has been an observed drying trend in this season (Funk et al., 2005, 2008; Liebmann et al., 2014; Maidment et al., 2015), which sharply contrasts the wetting predicted by most climate projections (Otieno & Anyah, 2013; Shongwe et al., 2011), often referred to as the "East African Climate Paradox" (Rowell et al., 2015). Some authors have demonstrated that the long rains decline is linked with natural decadal variability in the Pacific Ocean (Bahaga et al., 2019; Lyon, 2014; Yang et al., 2014), while others suggest anthropogenic factors (Funk & Hoell, 2015; Rowell et al., 2015; Williams & Funk, 2011). Meanwhile, recent work by Wainwright et al. (2019) has shown that over the Horn of Africa the observed long rains drying trend is caused by a shortening of the rainfall season and that in more recent years,

the long rains have begun to recover. Therefore, the future of the long rains is still highly uncertain. Improved understanding and prediction of variability in this season on interannual and decadal time scales, leading to improved rainfall forecasts, would be of great benefit to the local population.

Finney et al. (2019) recently demonstrated that although the climatological wind is easterly (Figure S1a in the supporting information), days with westerly winds originating from over the Congo basin do occur during the long rains season, and throughout the year. These events import moist air from over the Congo basin, causing convergence within the Lake Victoria basin, thereby leading to enhanced rainfall, with the record breaking 2018 long rains serving as a prime example (Kilavi et al., 2018). During MAM 2018 several westerly days occurred, linked to tropical cyclones in the Indian Ocean. Finney et al. (2019) also highlighted the role of the Madden-Julian Oscillation (MJO; Madden & Julian, 1971, 1972) influencing the formation of these tropical cyclones.

A more direct effect of MJO influence on the long rains has been documented by Pohl and Camberlin (2006a, 2006b). Pohl and Camberlin (2006a), using phases of the MJO defined by Wheeler and Hendon (2004), identified that Phases 2 and 3 from the Wheeler-Hendon index, when the convective core is over Africa and the Indian Ocean, were linked to increased rainfall over the East African highlands. Meanwhile, Vellinga and Milton (2018) demonstrated that a greater seasonal mean amplitude of the MJO as defined by Wheeler and Hendon (2004), regardless of phase, contributed to more abundant rainfall, due to an asymmetric response of the rainfall to the ascent/descent caused by specific phases.

While anomalous westerly wind influence over East Africa has been regularly described qualitatively in past literature (Camberlin & Wairoto, 1997; Diem et al., 2019; Nkunzimana et al., 2019; Okoola, 1999a, 1999b), little quantitative evidence for this had been presented until the work by Finney et al. (2019). Finney et al. (2019) showed the role of absolute westerlies for East African rainfall; this work uses this understanding to demonstrate the connection between zonal wind anomalies and East African rainfall on both interannual and decadal time scales, demonstrating a link between long-term change in the zonal winds over the Congo basin and the long rains drying trend (section 3.1), and also investigating explanations for variability of the zonal winds (section 3.2).

2. Data and Methods

The rainfall data for this study are Global Precipitation Climatology Project Version 2.3 (GPCP; Adler et al., 2003), while wind, geopotential height, and temperature data were obtained from European Centre for Medium-Range Weather Forecasts (ECMWF) Interim Reanalysis (ERA-Interim; Dee et al., 2011). MJO phase and amplitude data were obtained from the Bureau of Meteorology, where phase and amplitude are calculated using the method outlined in Wheeler and Hendon (2004), using National Oceanic and Atmospheric Administration (NOAA) outgoing long-wave radiation satellite observations (Liebmann & Smith, 1996), and National Centers for Environmental Prediction-National Center for Atmospheric Research (NCEP-NCAR; Kalnay et al., 1996) reanalysis winds. National Aeronautics and Space Administration (NASA) Modern Era Retrospective Analysis for Research and Applications, Version 2 (MERRA-2; Gelaro et al., 2017) winds and geopotential height data were used to verify relations between ERA-Interim variables and other observations.

This study uses the period 1979–2018, matching the satellite era and earliest available data from ERA-Interim and GPCP. Results were tested with the outlying year 2018 removed, with similar conclusions. The region considered for rainfall is highlighted in blue in Figure 1a, and future references to East Africa will refer to this region, while the zonal wind index is calculated as the mean 700 hPa zonal wind within 5°N to 5°S, 10°W to 30°E (brown box on Figures 1d and 1e).

Wet, dry, and recovery periods of the long rains, similar to those in Wainwright et al. (2019), are defined from 1979–1997 (P1), 1998–2011 (P2), and 2012–2018 (P3), respectively. Composites of the drying trend are considered using P2-P1. The wettest and driest years are calculated by fitting a cubic polynomial to the raw time series data, and then removing this, to remove long-term trends. The wettest and driest years within the long rains are defined as years where the rainfall total after trend removal is more than 0.8 standard deviations above and below the 1979–2018 seasonal mean, respectively. When discussing these sets of years, DECADAL will refer to the altered Wainwright periods (P2-P1), and INTERANNUAL will refer to the

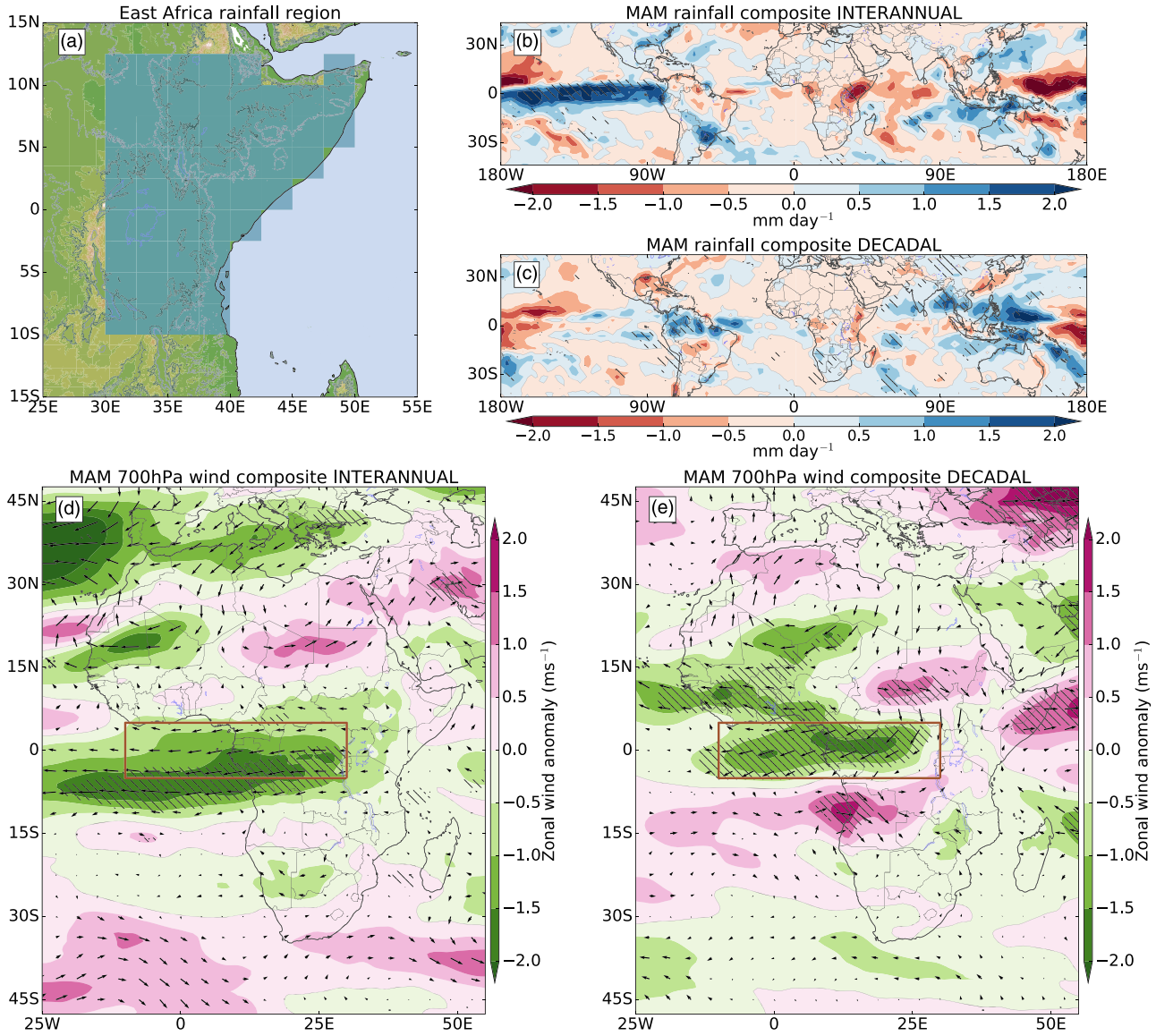

Figure 1. Interannual and decadal rainfall changes in East Africa. (a) East Africa rainfall region shaded blue (land within 12.5°N to 10°S, 30°E to 52.5°E), East Africa topography, colors, 500 and 1,000 m contours in light and dark gray. Composite of rainfall across the tropics during the long rains for (b) driest years minus wettest years, (c) dry period minus wet period (P2-P1). Composite of 700 hPa winds and zonal wind (colors) across Africa during the long rains for (d) driest years minus wettest years, (e) dry period minus wet period (P2-P1). Brown boxes show region used to calculate zonal wind index, hatching denotes areas where the composite values are significantly different from 0.

driest minus wettest years. Significance of trends were tested using the Mann-Kendall test, (Kendall, 1975; Mann, 1945), further details of which can be found in Wilks (2011).

The expected trend in mean rainfall between P1 and P2, $\Delta\bar{r}_{exp}$, due to the observed change in mean wind from P1 to P2, $\bar{u}_{P2} - \bar{u}_{P1}$, is given by

$$\Delta\bar{r}_{exp} = \frac{\mathrm{d}r}{\mathrm{d}u}(\bar{u}_{P2} - \bar{u}_{P1}) \quad (1)$$

where $\frac{\mathrm{d}r}{\mathrm{d}u}$ is the gradient of the regression of rainfall against wind after removing the polynomial fit. Variables r and u can be replaced by other variables. If $\Delta\bar{r}_{exp} \approx \Delta\bar{r}_{obs}$, where $\Delta\bar{r}_{obs}$ is the observed change in rainfall, then this is evidence that the mechanism that links rainfall and winds on interannual time scales can also explain the decadal variability in the rainfall.

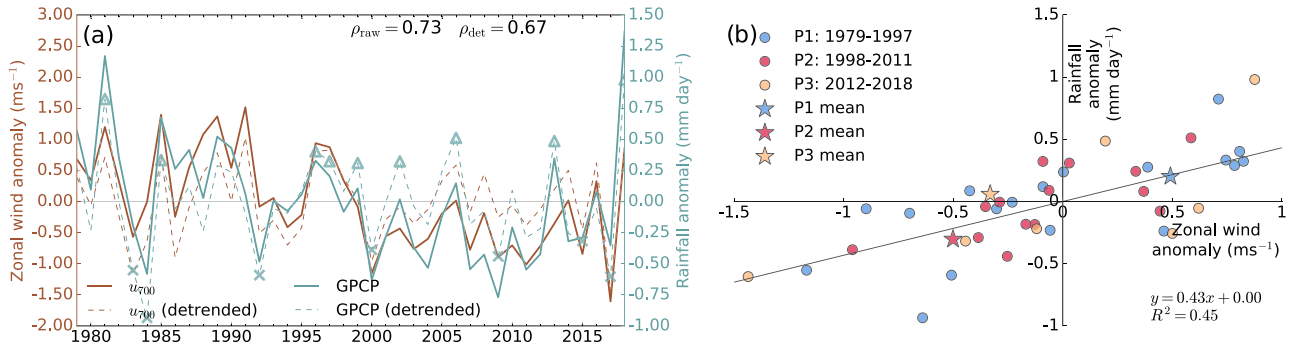

Figure 2. Temporal variations in East African rainfall and winds. (a) Time series of seasonal mean zonal wind anomaly (brown) and rainfall anomaly (blue) for boxes defined in Figure 1, dashed lines show time series after removing polynomial fit. The wet and dry years used for the INTERANNUAL composites are highlighted as triangles and crosses, respectively. Correlation values of zonal winds against rainfall, before and after detrending given in top right. (b) Scatter of zonal wind anomaly against rainfall anomaly after detrending, colored by P1 (blue), P2 (red), and P3 (yellow) periods. Black line is regression line fitted against the scatter, with regression equation and R^2 value given. Colored stars show mean anomaly of each period, with respect to 1979–2018 mean, before trend is removed.

3. Results

3.1. Interannual and Decadal Variability of the Long Rains

Figure 1 shows rainfall anomalies over the tropics and 700 hPa wind anomaly composites over Africa for INTERANNUAL and DECADAL. The 700 hPa level was chosen as it is largely above the topography of East Africa and was found to have the largest single-level moisture flux, and moisture flux anomaly in the INTERANNUAL composite (Figure S1b). In Figures 1b and 1c a dry signal is apparent over East Africa as expected, with wet anomalies over the Maritime Continent, and dry anomalies over the western Pacific, in a pattern reminiscent of the Pacific "V" discussed in Funk and Hoell (2015), Funk et al. (2019), and Lyon and Dewitt (2012). In Figures 1d and 1e a large easterly anomaly is present over the equatorial Atlantic Ocean and Congo basin. In INTERANNUAL, this extends to the Horn of Africa where it meets a westerly anomaly from the Indian Ocean, while in DECADAL this easterly anomaly is also present, but only reaches as far as the orography separating the Congo basin from East Africa. In DECADAL, the easterly anomalies appear to be linked to an anticyclonic anomaly over the Sahara desert; this level exhibits a midtropospheric high pressure, over the location of the summertime Saharan Heat Low (SHL), suggesting a stronger SHL in drier years (Evan et al., 2015). Heating and ascent in the SHL causes a low pressure near the surface and high pressure aloft at 700 hPa (Lavaysse et al., 2009; Rácz & Smith, 1999) and the 925 to 700 hPa thickness is directly proportional to the air temperature in the column. The 700 hPa anticyclone is therefore a useful measure of the SHL. The zonal wind anomaly (outlined by the brown box) is largely consistent with the findings of Finney et al. (2019), as an easterly anomaly in the seasonal mean is likely to contain less westerly, or weak easterly days. These results are insensitive to the reanalysis used, with similar patterns observed in equivalent MERRA-2 composites (Figures S2a and S2b).

Figure 2 shows the time series of the zonal wind index and long rains seasonal rainfall anomalies. A correlation between the rainfall and zonal winds of 0.73 is found, 0.67 with polynomial fits removed (both significant at the 1% level). This demonstrates the very strong connection between interannual variability in zonal wind and rainfall. This is again consistent in MERRA-2, with correlations of 0.81 (0.71 when detrended; Figure S2c). It is apparent from Figure 2a that both the rainfall and zonal wind demonstrate a decreasing trend, both significant at the 5% level, when treated linearly, using the Mann-Kendall trend test. Both variables show some signs of a recovery in P3, consistent with Wainwright et al. (2019). This is more apparent in the rainfall than winds in Figure 2a, while for MERRA-2 (Figure S2c) a recovery in the zonal winds is more visible.

Figure 2b shows the scatter of rainfall against zonal wind after detrending. The linear regression equation between the two variables is $r = 0.43u - 0.00$. From this, and from the linear trend of each variable, an expected trend of rainfall due to the observed trend in the zonal winds can be calculated (Equation 1). The expected change in mean rainfall from observed change in mean zonal wind from P1 to P2 is -0.43 ± 0.14 mm day^{-1}, the observed change is -0.50 ± 0.16 mm day^{-1}. These are statistically

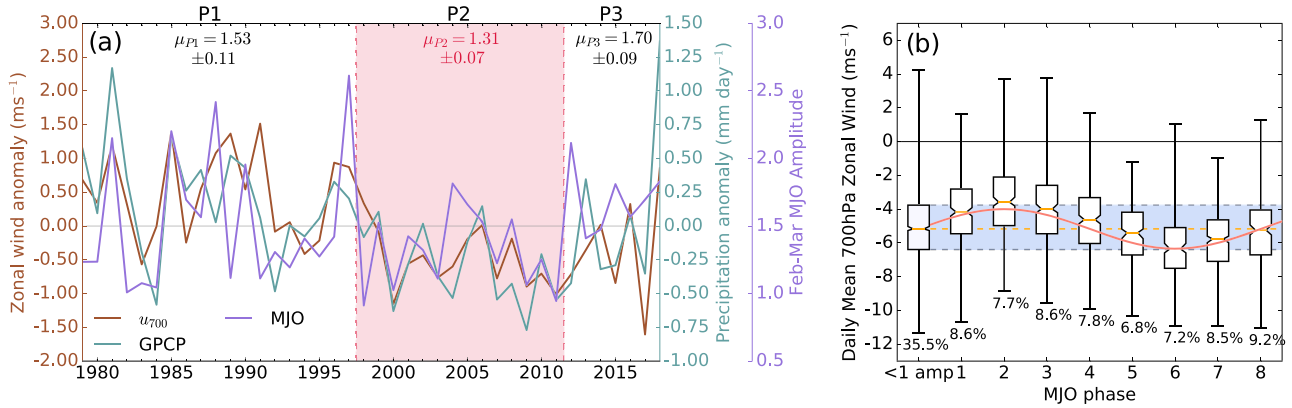

Figure 3. The MJO and East African rainfall. (a) Time series of zonal wind anomaly (brown) and rainfall anomaly (blue) as in Figure 2a, and February-March mean MJO amplitude (purple), means and standard errors of the MJO amplitudes during P1, P2, and P3 are given at the top, with periods separated by red dashed lines, and red shading over the dry period, P2. (b) Box plots of daily mean zonal wind separated by MJO phase, inactive days (MJO amplitude < 1) grouped in left box, notches on boxes show 95% confidence interval calculated from bootstrap resampling of 1,000 values, numbers below minimum of each box show percentage of days in that phase, blue shading shows interquartile range of inactive days, orange dashed line shows median of inactive days. Pink curve shows sine wave fitted to active days assuming a mean value equal to the median of the inactive days.

indistinguishable, so it is concluded that the observed decadal drying in the long rains can be largely explained by the same mechanism controlling the interannual relation between the zonal wind and rainfall.

While it is difficult to establish causality between the variability in the zonal winds and rainfall, and is likely the two operate in a coupled system, (Finney et al., 2019) provides a potential mechanism. By examining lagged relationships it is found that zonal winds early in the long rains (March) are more strongly correlated with rainfall later in the season (April-May), than the inverse (0.61 compared to 0.37). By also considering daily zonal winds against rainfall, it is found that the peak correlation occurs at 1 day lag (zonal wind of one day against rainfall of the next), and is found to be significantly higher than a 1 day lead correlation. Therefore, both monthly and daily analysis support wind anomalies leading to rainfall anomalies.

3.2. Drivers of Variability of the Zonal Winds

As the main conclusion of section 3.1 is that the zonal winds are strongly correlated with the long rains on the interannual time scale and can explain the decadal drying trend, an important question is to understand what is the controlling variability in these zonal winds on interannual and decadal time scales.

Recent work has shown the influence of the MJO amplitude on the long rains on interannual time scales (Pohl & Camberlin, 2006b; Vellinga & Milton, 2018). Figure 3a shows the time series of rainfall and zonal wind index alongside the February-March MJO amplitude used in Vellinga and Milton (2018). Correlation between MJO amplitude and zonal winds is 0.31, and between MJO and rainfall is 0.36 (0.34 and 0.35, respectively, when detrended). These fairly weak correlations are nevertheless significant at the 5% level, and correlations between MJO and zonal wind are stronger in MERRA-2 (0.48, 0.54 when detrended). In Figure 3a, there is significantly lower (at 5% level) mean MJO amplitude during P2 than P1 and P3. The mean MJO amplitude of P2 is 1.31 ± 0.07 while P1 and P3 are 1.53 ± 0.11 and 1.70 ± 0.09, respectively. The zonal wind index was regressed against the MJO amplitude (a), giving a regression equation of $u = 0.58a - 0.86$. The change in mean MJO amplitude from P1 to P2 is -0.21 ± 0.14, giving an expected change in mean zonal wind of -0.13 ± 0.07 m s^{-1} from Equation 1. The observed change in the zonal wind from P1 to P2 is -0.99 ± 0.26 m s^{-1}, meaning ~13% of the change in zonal wind can be attributed to the decrease in MJO amplitude. Similarly, regressing the rainfall against the MJO amplitude leads to an expected change of -0.09 ± 0.10 mm day^{-1}. The observed change in mean of the rainfall from P1 to P2 is -0.50 ± 0.14 mm day^{-1}, so ~18% of the change in rainfall can be attributed to the decrease in MJO amplitude.

Pohl and Camberlin (2006a) highlighted how different phases of the MJO influence winds around East Africa, some phases giving easterly anomalies, others westerly, so it is likely that by considering only amplitude these opposite influences mostly cancel out, accounting for the low correlations when amplitude alone is considered. However, if the wind response to phases is asymmetric, as for rainfall (Vellinga & Milton, 2018), this could explain the significant correlation, providing evidence that the MJO influences

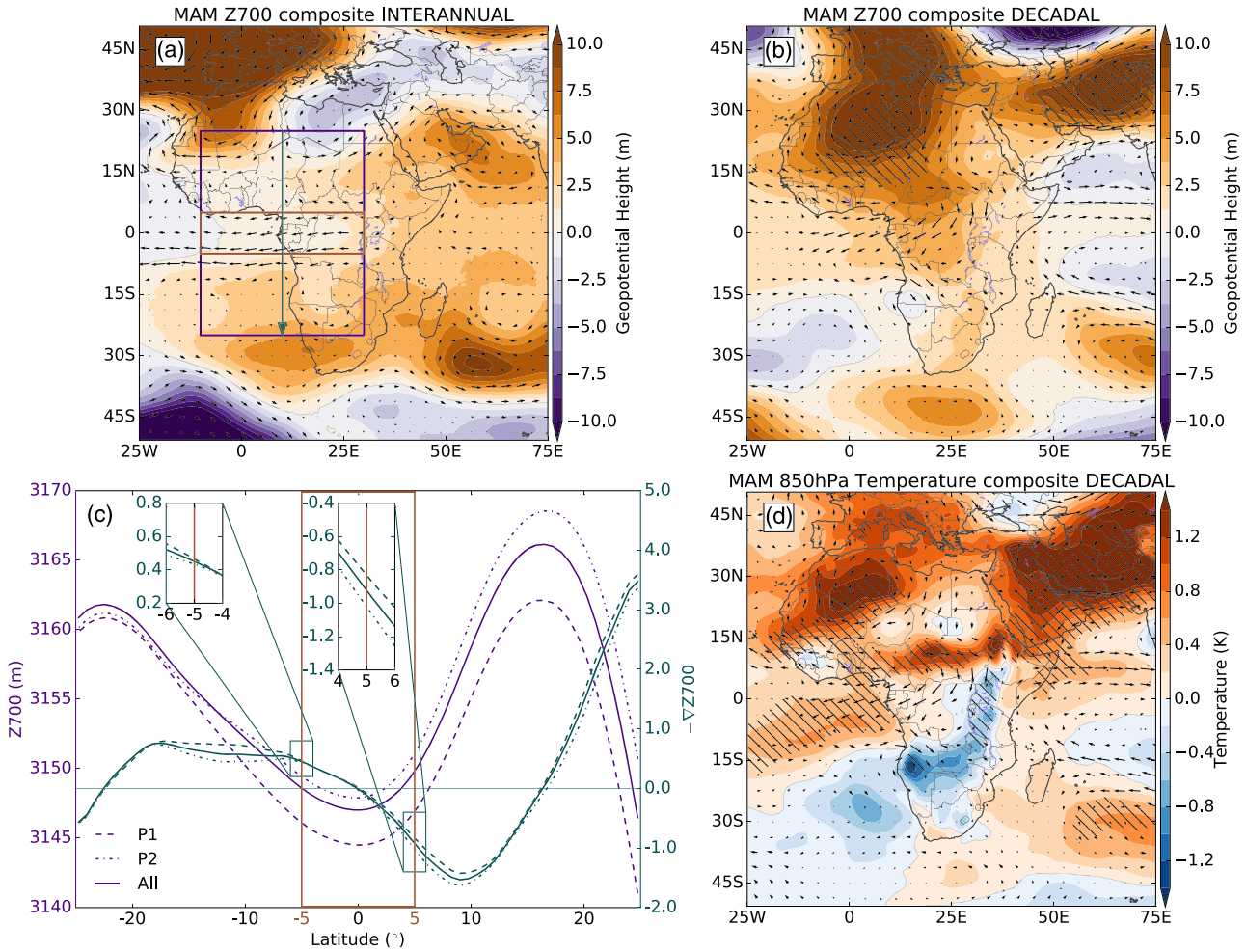

Figure 4. Interannual and decadal geopotential patterns over Africa. (a) Composites of 700 hPa geopotential height and winds for (a) INTERANNUAL, and (b), DECADAL. (c) Transect of mean geopotential height (purple) across each latitude for the purple box shown in (a), and gradient of the geopotential height (blue) multiplied by −1, following blue arrow shown in (a), for P1 (dashed), P2 (dotted), all years (solid). Inset boxes show geopotential gradients zoomed in to edges of zonal wind box (brown box). (d) 850 hPa temperature and 700 hPa winds for DECADAL, hatching denotes areas where the composite values are significantly different from 0.

interannual and decadal variability of the zonal winds. Alternatively, it may be that the mechanism driving variability in the zonal winds also impacts MJO amplitude. The effects of different phases of the MJO on the zonal winds and rainfall are considered. Figure 3b shows box and whisker diagrams of the daily mean of the zonal wind index, separated by MJO phase and separated into inactive days (amplitude < 1) and active days (amplitude > 1), in MAM. If the zonal winds of the inactive days are more strongly easterly than the active days, it can be concluded that the influence of the MJO on wind is asymmetric as discussed above. To determine this, it is assumed that the converse is true: the mean winds of active and inactive days are the same. A sinusoidal wave is fitted based on this assumption; however, the wind is overall less easterly than predicted by the curve, implying that the mean winds of active and inactive days are different. In particular, the phases reducing strength of easterlies (1–4) and also Phase 5, are less strongly easterly, while the phases increasing strength of easterlies lie roughly on the curve. To confirm this, taking the mean zonal wind of all active (-4.81 m s^{-1}), and inactive days (-5.02 m s^{-1}), and performing a one-sided t test, it is found that the mean zonal winds of active days are less easterly, significant at the 1% level (a similar but weaker result is found using MERRA-2, significant at the 5% level). Despite this asymmetry, it is still possible that rather than the MJO influencing the zonal winds (or vice versa), the correlation could result from a third process influencing both the MJO amplitude and zonal winds separately.

While the MJO can explain some of the interannual and decadal variability of the zonal winds, the fairly weak correlation and low percentage of explained change in mean suggests that other factors must be

involved. Figure 4 shows dry minus wet composites of geopotential height at 700 hPa (Z700), for INTERANNUAL and DECADAL. In both the INTERANNUAL and DECADAL the 700 hPa wind anomalies follow closely the gradients in anomaly in Z700, as expected. Figure 4c also shows the 850 hPa temperature for DECADAL. By the hypsometric equation, the geopotential thickness between two layers is directly proportional to the mean temperature within them, and this composite is therefore similar to the geopotential thickness between 700 and 925 hPa (not shown).

In the INTERANNUAL composite (Figure 4a), there is a geopotential anomaly over the eastern Sahel, extending over Arabia. This area is also where both geopotential thickness and Z700 are maximal in the climatology (Figures S1c and S1d). Therefore, in dry years, the maxima in geopotential thickness and Z700 are increased, causing a larger meridional geopotential gradient from the Sahel to the Congo, consistent with increased strength of easterly winds.

In the DECADAL composites (Figures 4c and 4d), there are large similarities between the composites of Z700 and 850 hPa temperature. An anomaly over the eastern Sahel, as in Figure 4a also stands out in both of these, with positive anomalies, reducing in magnitude from 15°N southward through the equator. This again gives an increased geopotential gradient at 700 hPa, consistent with increased strength of easterly winds. Two large anomalies stand out over the west Sahara and Arabian peninsula. These are the approximate locations of the summertime SHL and Arabian Heat Low (AHL). The 700–925 hPa geopotential thickness is a common measure of the strength of the SHL, as defined by Lavaysse et al. (2009), implying that both the SHL and AHL have increased in strength.

Figure 4c shows the latitudinally averaged Z700 across the purple box in Figure 4a, and latitudinal gradient of Z700 multiplied by −1 over this region, for P1, P2, and all years. An increase in Z700 across the region in P2 compared with P1 is evident. There is also a maximum (trough) in the gradient at roughly 10°N, with P2 displaying a stronger maximum. This causes a stronger gradient on the north side of the zonal wind box (5°N: right inset of Figure 4c) while at the southern edge of the box (5°S: left inset of Figure 4c) such a pattern is absent. This shows that the increased meridional geopotential gradient across the zonal wind box is related to the increased geopotential gradient to the north, from the increasingly strong maximum in the Z700 in the eastern Sahel. This is also apparent in MERRA-2 (Figure S2d). In Figure 4d, from P1 to P2, the increase in temperature (and geopotential thickness) is driven by a more rapidly warming eastern Sahel and west Sahara, than over the Congo basin, increasing the meridional geopotential gradient at 700 hPa, with increasingly strong easterly winds over the Congo region and drier East Africa.

Another possible mechanism could be analogous to equatorial superrotation (Dima et al., 2005; Kraucunas & Hartmann, 2005; Yang et al., 2013). Rainfall is associated with organized convection which can excite Rossby wave propagation and convergence of zonal momentum to the source of the disturbances. Further, any regional wind change influences divergence; an easterly anomaly to the west, reducing in magnitude eastward, produces a decrease in moisture flux convergence over East Africa. However this alone is not enough to imply that the zonal winds drive rainfall, as anomalous heating from rainfall can also feed back onto local convergence and circulation.

4. Discussion and Conclusions

This study has investigated the relationship between 700 hPa zonal winds across the Gulf of Guinea and Congo basin, and rainfall during the East African long rains. It was found that the seasonal mean 700 hPa zonal wind over this area is strongly correlated with long rains rainfall totals ($r = 0.73$). Considering periods similar to Wainwright et al. (2019), with a wet (P1: 1979–1997), dry (P2: 1998–2011), and recovery period (P3: 2012–2018), it was found that the same relationship is seen on decadal time scales (P2-P1), showing the importance of the zonal winds to East African climate paradox drying. Meanwhile, a recovery during P3, in agreement with Wainwright et al. (2019), is seen not only in rainfall but also in the zonal winds. The mechanism linking the zonal winds to rainfall on interannual time scales is found to quantitatively explain the long rains drying trend through the decreasing trend in the zonal winds.

The mechanism driving variability in the zonal winds was explored, with some contribution coming from the MJO amplitude, both on interannual and decadal time scales, with wind response to MJO by phase being subtly asymmetric, as seen for rainfall (Vellinga & Milton, 2018). There was a significantly weaker MJO amplitude during P2, accounting for 18% and 13% of the decline in rainfall and wind, respectively.

Meanwhile, another mechanism for the interannual and decadal variability was shown considering changes in geopotential gradients. For interannual variability, these lead to stronger easterlies in drier years due to higher geopotential height over the eastern Sahel, caused by increased warming here, strengthening the geopotential gradient. For decadal variability, a similar mechanism is present but is also aligned to increased heating around Arabia and Sahara regions.

What has not been explored is the source of differing rates of warming between the Sahel and the Congo basin. During the study period, a decadal decline in rainfall over Arabia has been reported (Almazroui et al., 2012), excess heating during this period could be linked to a decadal trend in dust activity over the Arabian Peninsula (Yu et al., 2015), that is also causing a strengthening AHL (Solmon et al., 2015). Wainwright et al. (2019) linked a deepening AHL to faster progression of the tropical rainband over East Africa during the long rains, shortening the season, and Dunning et al. (2018) links a deepening SHL under climate change to a delayed return of the rainband southward in boreal autumn. This motivates further investigation into variations in seasonal Hadley Cell migration, and the associated impacts on zonal flow. The eastern Sahel and Arabia region has experienced a rapid, almost step-like change in temperature around the end of P1 (Almazroui et al., 2012; Attada et al., 2018; Hu et al., 2019; Taylor et al., 2018). The amplified Saharan change in temperature is linked to the observed deepening of the SHL, also responsible for the partial recovery of the Sahelian drought (Evan et al., 2015). Thus the SHL plays two key roles: affecting monsoon onset/ retreat and the latitudinal progression of the rain band (Dunning et al., 2018; Lavaysse et al., 2009), and as shown here by affecting zonal winds across central Africa, which are important for water vapor transport and East African rainfall (Finney et al., 2019). Further strengthening of the SHL is expected under climate change (Biasutti et al., 2009; Dong & Sutton, 2015), which through the above mechanisms could lead to further drying of the long rains.

Based on these results, further understanding of how relative warming rates might change in the future could provide an alternative viewpoint into the future of the long rains through changes in regional dynamics (also supported by Kent et al., 2015). For example, Giannini et al. (2018) demonstrated that in the Coupled Model Intercomparison Project phase 5 (CMIP5; Taylor et al., 2012), a mechanism consistent with wetter years shown here is present during MAM, with moisture advected away from the Congo toward East Africa, linked to a slower overturning circulation under climate change.

While in the long rains, sea surface temperatures (SSTs) are less well connected to rainfall totals than in the short rains, weaker, but significant, relations do exist on both interannual (Ogallo, 1988; Vellinga & Milton, 2018), and longer-term (Bahaga et al., 2019; Liebmann et al., 2014; Williams & Funk, 2011) time scales. Understanding how the processes discussed here are influenced by SSTs could determine their predictability. Given that these zonal winds are of great importance to variability within the long rains, it should be a priority to investigate whether forecast models are able to capture this relationship. This could improve seasonal forecasting and provide useful information on the potential future of the long rains.

Acknowledgments
This work was supported by the Natural Environment Research Council (NERC) through an industrial CASE award with the UK Met Office (grant NE/N008227/1). Marsham and Finney were supported by the HyCRISTAL project (grant NE/M02038X/1). Birch and Marsham were supported by the UK Research and Innovation as part of the Global Challenges Research Fund, grant number NE/P021077/1 (GCRF African SWIFT). Marsham was also supported by the NCAS ACREW project. Scaife was supported by the Joint DECC/Defra Met Office Hadley Centre Climate Programme (GA01101), and by the Met Office Hadley Centre Climate Programme funded by BEIS and Defra. The authors would like to thank Michael Vellinga and Dave Rowell for their helpful discussions. The authors would like to thank the reviewers for their comments, which have helped to improve the quality and clarity of the manuscript.

Data Availability Statement

All data used in this study can be freely downloaded from the following locations: GPCP data were provided by NOAA/ESRL PSD (www.esrl.noaa.gov/psd/data/gridded/data.gpcp.html) ERA-Interim Reanalysis data were provided by ECMWF (www.ecmwf.int/en/forecasts/datasets/reanalysis-datasets/era-interim). MERRA-2 was provided by the Global Modeling and Assimilation Office, NASA (gmao.gsfc.nasa.gov/reanalysis/MERRA-2/). Daily MJO Index data were provided by the Bureau of Meteorology, Melbourne, Australia (www.bom.gov.au/climate/mjo).

References

Adler, R. F., Huffman, G. J., Chang, A., Ferraro, R., Xie, P.-P., Janowiak, J., et al. (2003). The Version-2 Global Precipitation Climatology Project (GPCP) monthly precipitation analysis (1979-Present). *Journal of Hydrometeorology*, *4*(6), 1147–1167. https://doi.org/10.1175/1525-7541(2003)004<1147:TVGPCP>2.0.CO;2

Almazroui, M., Islam, M. N., Jones, P. D., Athar, H., & Rahman, M. A. (2012). Recent climate change in the Arabian Peninsula: Seasonal rainfall and temperature climatology of Saudi Arabia for 1979–2009. *Atmospheric Research*, *111*, 29–45. https://doi.org/10.1016/j.atmosres.2012.02.013

Attada, R., Dasari, H. P., Chowdary, J. S., Yadav, R. K., Knio, O., & Hoteit, I. (2018). Surface air temperature variability over the Arabian Peninsula and its links to circulation patterns. *International Journal of Climatology*, *39*(1), 445–464. https://doi.org/10.1002/joc.5821

Bahaga, T. K., Fink, A. H., & Knippertz, P. (2019). Revisiting interannual to decadal teleconnections influencing seasonal rainfall in the Greater Horn of Africa during the 20th century. *International Journal of Climatology*, *39*(5), 2765–2785. https://doi.org/10.1002/joc.5986

Batté, L., & Déqué, M. (2011). Seasonal predictions of precipitation over Africa using coupled ocean-atmosphere general circulation models: Skill of the ENSEMBLES project multimodel ensemble forecasts. *Tellus, Series A: Dynamic Meteorology and Oceanography*, *63A*(2), 283–299. https://doi.org/10.1111/j.1600-0870.2010.00493.x

Biasutti, M., Sobel, A. H., & Camargo, S. J. (2009). The role of the Sahara low in summertime Sahel rainfall variability and change in the CMIP3 models. *Journal of Climate*, *22*(21), 5755–5771. https://doi.org/10.1175/2009JCLI2969.1

Black, E., Slingo, J., & Sperber, K. R. (2003). An observational study of the relationship between excessively strong short rains in coastal East Africa and Indian Ocean SST. *Monthly Weather Review*, *131*(1), 74–94. https://doi.org/10.1175/1520-0493(2003)131<0074:AOSOTR>2.0.CO;2

Camberlin, P., & Philippon, N. (2002). The East African March-May rainy season: Associated atmospheric dynamics and predictability over the 1968–97 period. *Journal of Climate*, *15*(9), 1002–1019. https://doi.org/10.1175/1520-0442(2002)015<1002:TEAMMR>2.0.CO;2

Camberlin, P., & Wairoto, J. G. (1997). Intraseasonal wind anomalies related to wet and dry spells during the "long" and "short" rainy seasons in Kenya. *Theoretical and Applied Climatology*, *58*(1–2), 57–69. https://doi.org/10.1007/BF00867432

Dee, D. P., Uppala, S. M., Simmons, A. J., Berrisford, P., Poli, P., Kobayashi, S., et al. (2011). The ERA-Interim reanalysis: Configuration and performance of the data assimilation system. *Quarterly Journal of the Royal Meteorological Society*, *137*(656), 553–597. https://doi.org/10.1002/qj.828

Diem, J. E., Sung, H. S., Konecky, B. L., Palace, M. W., Salerno, J., & Hartter, J. (2019). Rainfall characteristics and trends and the role of Congo westerlies in the western Uganda transition zone of equatorial Africa from 1983 to 2017. *Journal of Geophysical Research: Atmospheres*, *124*, 10,712–10,729. https://doi.org/10.1029/2019JD031243

Dima, I. M., Wallace, J. M., & Kraucunas, I. (2005). Tropical zonal momentum balance in the NCEP reanalyses. *Journal of the Atmospheric Sciences*, *62*(7 II), 2499–2513. https://doi.org/10.1175/JAS3486.1

Dong, B., & Sutton, R. (2015). Dominant role of greenhouse-gas forcing in the recovery of Sahel rainfall. *Nature Climate Change*, *5*(8), 757–760. https://doi.org/10.1038/nclimate2664

Dunning, C. M., Black, E., & Allan, R. P. (2018). Later wet seasons with more intense rainfall over Africa under future climate change. *Journal of Climate*, *31*(23), 9719–9738. https://doi.org/10.1175/JCLI-D-18-0102.1

Dutra, E., Magnusson, L., Wetterhall, F., Cloke, H. L., Balsamo, G., Boussetta, S., & Pappenberger, F. (2013). The 2010–2011 drought in the Horn of Africa in ECMWF reanalysis and seasonal forecast products. *International Journal of Climatology*, *33*(7), 1720–1729. https://doi.org/10.1002/joc.3545

Evan, A. T., Flamant, C., Lavaysse, C., Kocha, C., & Saci, A. (2015). Water vapor-forced greenhouse warming over the Sahara desert and the recent recovery from the Sahelian drought. *Journal of Climate*, *28*(1), 108–123. https://doi.org/10.1175/JCLI-D-14-00039.1

Finney, D. L., Marsham, J. H., Walker, D. P., Birch, C. E., Woodhams, B. J., Jackson, L. S., & Hardy, S. (2019). The effect of westerlies on East African rainfall and the associated role of tropical cyclones and the Madden-Julian Oscillation. *Quarterly Journal of the Royal Meteorological Society*, *146*, 647–664. https://doi.org/10.1002/qj.3698

Funk, C. C., Dettinger, M. D., Michaelsen, J. C., Verdin, J. P., Brown, M. E., Barlow, M., & Hoell, A. (2008). Warming of the Indian Ocean threatens eastern and southern African food security but could be mitigated by agricultural development. *Proceedings of the National Academy of Sciences*, *105*(32), 11,081–11,086. https://doi.org/10.1073/pnas.0708196105

Funk, C. C., & Hoell, A. (2015). The leading mode of observed and CMIP5 ENSO-residual sea surface temperatures and associated changes in Indo-Pacific climate. *Journal of Climate*, *28*(11), 4309–4329. https://doi.org/10.1175/JCLI-D-14-00334.1

Funk, C. C., Pedreros, D., Nicholson, S., Hoell, A., Korecha, D., Galu, G., et al. (2019). Examining the potential contributions of extreme Western V sea surface temperatures to the 2017 March-June East African drought. *Bulletin of the American Meteorological Society*, *100*(1), S55–S60. https://doi.org/10.1175/BAMS-D-18-0108.1

Funk, C. C., Senay, G., Asfaw, A., & Verdin, J. (2005). Recent drought tendencies in Ethiopia and equatorial-subtropical eastern Africa. FEWS NET Special Report.

Gelaro, R., McCarty, W., Suárez, M. J., Todling, R., Molod, A., Takacs, L., et al. (2017). The Modern-Era Retrospective Analysis for research and applications, version 2 (MERRA-2). *Journal of Climate*, *30*(14), 5419–5454. https://doi.org/10.1175/JCLI-D-16-0758.1

Giannini, A., Lyon, B., Seager, R., & Vigaud, N. (2018). Dynamical and thermodynamic elements of modeled climate change at the East African margin of convection. *Geophysical Research Letters*, *45*, 992–1000. https://doi.org/10.1002/2017GL075486

Hu, L., Luo, J.-J., Huang, G., & Wheeler, M. C. (2019). Synoptic features responsible for heat waves in Central-Africa, a region with strong multi-decadal trend. *Journal of Climate*, *32*(22), 7951–7970. https://doi.org/10.1175/jcli-d-18-0807.1

Indeje, M., Semazzi, F. H. M., & Ogallo, L. J. (2000). ENSO signals in East African rainfall seasons. *International Journal of Climatology*, *20*(1), 19–46. https://doi.org/10.1002/(SICI)1097-0088(200001)20:1<19::AID-JOC449>3.0.CO;2-0

Kalnay, E., Kanamitsu, M., Kistler, R., Collins, W., Deaven, D., Gandin, L., et al. (1996). The NCEP/NCAR 40-year reanalysis project. *Bulletin of the American Meteorological Society*, *77*(3), 437–472. https://doi.org/10.1175/1520-0477(1996)077<0437:TNYRP>2.0.CO;2

Kendall, M. G. (1975). *Rank correlation methods* (4th ed.). London: Charles Griffin.

Kent, C., Chadwick, R., & Rowell, D. P. (2015). Understanding uncertainties in future projections of seasonal tropical precipitation. *Journal of Climate*, *28*(11), 4390–4413. https://doi.org/10.1175/JCLI-D-14-00613.1

Kilavi, M., MacLeod, D., Ambani, M., Robbins, J., Dankers, R., Graham, R., et al. (2018). Extreme rainfall and flooding over central Kenya including Nairobi city during the long-rains season 2018: Causes, predictability, and potential for early warning and actions. *Atmosphere*, *9*(12), 472. https://doi.org/10.3390/atmos9120472

Kraucunas, I., & Hartmann, D. L. (2005). Equatorial superrotation and the factors controlling the zonal-mean zonal winds in the tropical upper troposphere. *Journal of the Atmospheric Sciences*, *62*(2), 371–389. https://doi.org/10.1175/JAS-3365.1

Lavaysse, C., Flamant, C., Janicot, S., Parker, D. J., Lafore, J. P., Sultan, B., & Pelon, J. (2009). Seasonal evolution of the West African heat low: A climatological perspective. *Climate Dynamics*, *33*(2-3), 313–330. https://doi.org/10.1007/s00382-009-0553-4

Liebmann, B., Hoerling, M. P., Funk, C. C., Bladé, I., Dole, R. M., Allured, D., et al. (2014). Understanding recent eastern Horn of Africa rainfall variability and change. *Journal of Climate*, *27*(23), 8630–8645. https://doi.org/10.1175/JCLI-D-13-00714.1

Liebmann, B., & Smith, C. A. (1996). Description of a complete (interpolated) outgoing longwave radiation dataset. *Bulletin of the American Meteorological Society*, *77*(6), 1275–1277.

Lyon, B. (2014). Seasonal drought in the Greater Horn of Africa and its recent increase during the March-May long rains. *Journal of Climate*, *27*(21), 7953–7975. https://doi.org/10.1175/JCLI-D-13-00459.1

Lyon, B., & Dewitt, D. G. (2012). A recent and abrupt decline in the East African long rains. *Geophysical Research Letters*, *39*, L02702. https://doi.org/10.1029/2011GL050337

Madden, R. A., & Julian, P. R. (1971). Detection of a 40–50 day oscillation in the zonal wind in the tropical Pacific. *Journal of the Atmospheric Sciences*, *28*(5), 702–708. https://doi.org/10.1175/1520-0469(1971)028<0702:DOADOI>2.0.CO;2

Madden, R. A., & Julian, P. R. (1972). Description of global-scale circulation cells in the tropics with a 40–50 day period. *Journal of the Atmospheric Sciences*, *29*(6), 1109–1123. https://doi.org/10.1175/1520-0469(1972)029<1109:DOGSCC>2.0.CO;2

Maidment, R. I., Allan, R. P., & Black, E. (2015). Recent observed and simulated changes in precipitation over Africa. *Geophysical Research Letters*, *42*, 8155–8164. https://doi.org/10.1002/2015GL065765

Mann, H. B. (1945). Nonparametric tests against trend. *Econometrica*, *13*(3), 245–259.

Nicholson, S. E. (2017). Climate and climatic variability of rainfall over eastern Africa. *Reviews of Geophysics*, *55*, 590–635. https://doi.org/10.1002/2016RG000544

Nicholson, S. E., & Entekhabi, D. (1986). The quasi-periodic behavior of rainfall variability in Africa and its relationship to the southern oscillation. *Archives for Meteorology, Geophysics, and Bioclimatology Series A*, *34*(3–4), 311–348. https://doi.org/10.1007/BF02257765

Nkunzimana, A., Bi, S., Jiang, T., Wu, W., & Abro, M. I. (2019). Spatiotemporal variation of rainfall and occurrence of extreme events over Burundi during 1960 to 2010. *Arabian Journal of Geosciences*, *12*, 176. https://doi.org/10.1007/s12517-019-4335-y

Ogallo, L. J. (1988). Relationships between seasonal rainfall in East Africa and the Southern Oscillation. *Journal of Climatology*, *8*(1), 31–43. https://doi.org/10.1002/joc.3370080104

Okoola, R. E. (1999a). A diagnostic study of the eastern Africa monsoon circulation during the northern hemisphere spring season. *International Journal of Climatology*, *19*(2), 143–168. https://doi.org/10.1002/(SICI)1097-0088(199902)19:2<143::AID-JOC342>3.0.CO;2-U

Okoola, R. E. (1999b). Midtropospheric circulation patterns associated with extreme dry and wet episodes over equatorial Eastern Africa during the Northern Hemisphere spring. *Journal of Applied Meteorology*, *38*(8), 1161–1169. https://doi.org/10.1175/1520-0450(1999)038<1161:MCPAWE>2.0.CO;2

Otieno, V. O., & Anyah, R. O. (2013). CMIP5 simulated climate conditions of the Greater Horn of Africa (GHA). Part II: Projected climate. *Climate Dynamics*, *41*(7–8), 2099–2113. https://doi.org/10.1007/s00382-013-1694-z

Pohl, B., & Camberlin, P. (2006a). Influence of the Madden-Julian Oscillation on East African rainfall. I: Intraseasonal variability and regional dependency. *Quarterly Journal of the Royal Meteorological Society*, *132*(621), 2521–2539. https://doi.org/10.1256/qj.05.223

Pohl, B., & Camberlin, P. (2006b). Influence of the Madden-Julian Oscillation on East African rainfall. II: March-May season extremes and interannual variability. *Quarterly Journal of the Royal Meteorological Society*, *132*(621), 2541–2558. https://doi.org/10.1256/qj.05.104

Rácz, Z., & Smith, R. K. (1999). The dynamics of heat lows. *Quarterly Journal of the Royal Meteorological Society*, *125*(533), 225–252. https://doi.org/10.1002/qj.49712555313

Rowell, D. P., Booth, B. B. B., Nicholson, S. E., & Good, P. (2015). Reconciling past and future rainfall trends over East Africa. *Journal of Climate*, *28*(24), 9768–9788. https://doi.org/10.1175/JCLI-D-15-0140.1

Saji, N. H., Goswami, B. N., Vinayachandran, P. N., & Yamagata, T. (1999). A dipole mode in the tropical Indian Ocean. *Nature*, *401*(6751), 360–363. https://doi.org/10.1038/43854

Shongwe, M. E., van Oldenborgh, G. J., van den Hurk, B., & van Aalst, M. (2011). Projected changes in mean and extreme precipitation in Africa under global warming. Part II: East Africa. *Journal of Climate*, *24*(14), 3718–3733. https://doi.org/10.1175/2010JCLI2883.1

Solmon, F., Nair, V. S., & Mallet, M. (2015). Increasing Arabian dust activity and the Indian summer monsoon. *Atmospheric Chemistry and Physics*, *15*(14), 8051–8064. https://doi.org/10.5194/acp-15-8051-2015

Taylor, C. M., Fink, A. H., Klein, C., Parker, D. J., Guichard, F., Harris, P. P., & Knapp, K. R. (2018). Earlier seasonal onset of intense mesoscale convective systems in the Congo basin since 1999. *Geophysical Research Letters*, *45*, 13,458–13,467. https://doi.org/10.1029/2018GL080516

Taylor, K. E., Stouffer, R. J., & Meehl, G. A. (2012). An overview of CMIP5 and the experiment design. *Bulletin of the American Meteorological Society*, *93*(4), 485–498. https://doi.org/10.1175/BAMS-D-11-00094.1

Vellinga, M., & Milton, S. F. (2018). Drivers of interannual variability of the East African 'Long Rains'. *Quarterly Journal of the Royal Meteorological Society*, *144*, 861–876. https://doi.org/10.1002/qj.3263

Wainwright, C. M., Marsham, J. H., Keane, R. J., Rowell, D. P., Finney, D. L., Black, E., & Allan, R. P. (2019). 'Eastern African Paradox' rainfall decline due to shorter not less intense Long Rains. *npj Climate and Atmospheric Science*, *2*(1), 1–9. https://doi.org/10.1038/s41612-019-0091-7

Walker, D. P., Birch, C. E., Marsham, J. H., Scaife, A. A., Graham, R. J., & Segele, Z. T. (2019). Skill of dynamical and GHACOF consensus seasonal forecasts of East African rainfall. *Climate Dynamics*, *53*(7), 4911–4935. https://doi.org/10.1007/s00382-019-04835-9

Wheeler, M. C., & Hendon, H. H. (2004). An all-season real-time multivariate MJO Index: Development of an index for monitoring and prediction. *Monthly Weather Review*, *132*(8), 1917–1932. https://doi.org/10.1175/1520-0493(2004)132<1917:AARMMI>2.0.CO;2

Wilks, D. S. (2011). *Statistical methods in the atmospheric sciences* (3rd ed.). Oxford: Elsevier.

Williams, A. P., & Funk, C. C. (2011). A westward extension of the warm pool leads to a westward extension of the Walker circulation, drying eastern Africa. *Climate Dynamics*, *37*(11–12), 2417–2435. https://doi.org/10.1007/s00382-010-0984-y

Yang, W., Seager, R., & Cane, M. A. (2013). Zonal momentum balance in the tropical atmospheric circulation during the global monsoon mature months. *Journal of the Atmospheric Sciences*, *70*(2), 583–599. https://doi.org/10.1175/JAS-D-12-0140.1

Yang, W., Seager, R., Cane, M. A., & Lyon, B. (2014). The East African long rains in observations and models. *Journal of Climate*, *27*(19), 7185–7202. https://doi.org/10.1175/JCLI-D-13-00447.1

Yu, Y., Notaro, M., Liu, Z., Wang, F., Alkolibi, F., Fadda, E., & Bakhrjy, F. (2015). Climatic controls on the interannual to decadal variability in Saudi Arabian dust activity: Toward the development of a seasonal dust prediction model. *Journal of Geophysical Research: Atmospheres*, *120*, 1739–1758. https://doi.org/10.1002/2014JD022611